Analysis of Seismic Data Compression Using SPIHT in Seismic Inversion

Victor Martins Gomes[1]*; Marco Antonio Cetale Santos[1]; Rodrigo Bird Burgos[2];
[1]Departamento de Geologia e Geofísica, Instituto de Geociências, Universidade Federal Fluminense
[2]Departamento de Estruturas e Fundações, Universidade Estadual do Rio de Janeiro

ABSTRACT

This work aims to analyse how seismic data compression affect the acoustic impedance estimative. First data is compressed with the SPIHT method considering three values for reduction in the bit per pixel representation. Latter the compressed data is reconstructed and inverted by using the same parameters used in the original data and an inversion method based in the Levenberg-Marquardt algorithm. Results of compression and inversion are analyzed from a qualitative point of view, by analyzing the visual quality of the compressed data and quantitative by measuring the percentage of energy from the compressed data to the original data and the percentage of data compression, for results from the first, and the root mean squared error and the peak signal-to-noise ratio, for results from both.

INTRODUCTION

Exploration, evaluation and monitoring of hydrocarbon reservoirs uses as its main source of information about the subsurface, seismic data. However, with the increasing need of hydrocarbons, a large amount of seismic data was acquired. The storage of these data becomes a problem when a single data acquisition can have a Terabytes size. In this context, the seismic data compression becomes an important step, ensuring that more data can be stored while using less space.

Several seismic data compression methods currently exists in the literature. Most of them make use of the wavelet transform along with some threshold technique of the wavelet transformed coefficients as in Luo and Schuster (1992), Villasenor et al. (1996) and Zheludev et al. (2004).

Compression methods can be classified as lossy, when there is some loss of information, or losless, when all the information can be restored. For lossy methods, it is desired that errors be as minimal as possible, considering a threshold.

A commonly used technique to contribute in seismic interpretation is seismic inversion. Data inversion involves a mathematical treatment of seismic sections, therefore the less uncertainty (less error, noise, etc.) in the data, the better will the estimated subsurface model be. Hence, for seismic data, uncertainty in compression is directed related to uncertaninty in inversion.

In this work, seismic inversion works as a quantitative analysis of data compression. The compressive method used was the SPIHT (Said and Pearlman, 1996), considering data wavelet transformed.

For inversion of the seismic data Levenberg-Marquardt's method, described in Levenberg (1944) and Marquardt (1963), and as proposed by Cooke and Schneider (1983), was adopted.

A seismic volume from the Marimba oil field, with 101 inlines and 201 crosslines, and three wells from the area were used for analysis.

METODOLOGY

The methodology followed in this work follows: First transform the data to wavelet domain, second compress the seismic data volume using SPIHT at different compression rates, third invert the data and at last, analyse how the inversion results are affected by compression.

Wavelet Tansform

The wavelet transform (WT) involves a multiresolution analysis of a signal by expanding it in relation to a wavelet function basis (one scale and one wavelet or detail function), the same way Fourier transforming expands a signal in relation to an orthogonal basis of sinusoids (sines and cosines). However, unlike the Fourier transform, wavelet transforming allows signal representation not only in the frequency domain, but also provides temporal information (or space depending on the application field), hence enabling a local analysis of signal variations admitting various resolution levels (Burgos et al., 2013).

Through the multiresolution analysis concept introduced in Mallat (1989) and the nested condition of the wavelet basis functions, the scale function can be represented as a weighted sum of translated versions of itself scaled by a factor 2, as shown in the equation below:

$$\nu(t) = \sum_n h_{lp}\sqrt{2}\,\nu(2t-n), \quad n \in \mathcal{Z}. \tag{1}$$

Coefficients h_{lp} above are related to the known analysis low-pass filter and $\sqrt{2}$ normalizes the scale function by a factor 2. In addition, the wavelet function can be represented by a weighted sum of translated version of the scale function dilated by a factor 2.

$$\upsilon(t) = \sum_n h_{hp}\sqrt{2}\,\nu(2t-n), \quad n \in \mathcal{Z}. \tag{2}$$

Coefficients h_{hp} relate to the known analysis high-pass filter.

When working with seismic data, images, digital signals in general, it is not necessary to work directly with scale or wavelets functions. In this case what should be considered is the analysis and reconstruction filters

and the approximation and detail coefficients, which can be regarded as digital filters and signals, respectively (Vaidyanathan, 1993). In general, analysis (decomposition) and reconstruction (synthesis) of a signal can be represented as two two-channel filter banks (Mertins, 1999), as shown in figure 1.

$$c_j(k) = \sum_m h_{lp}(m-2k)c_{(j+1)}(m) \tag{3a}$$

$$d_j(k) = \sum_m h_{hp}(m-2k)c_{(j+1)}(m) \tag{3b}$$

$$c_{(j+1)}(k) = \sum_m c_j(m)g_{lp}(k-2m) + \\ + \sum_m d_j(m)g_{hp}(k-2m) \tag{3c}$$

By looking at the equations above, it can be noticed that in the analysis step, approximation and detail coefficients at resolution scale j can be calculated through convolution of coefficients at scale $j+1$ with filters $h_{lp}(-n)$ and $h_{hp}(-n)$ followed by decimation with a factor 2 (preserving only the even terms). Thus the analysed signal is decomposed into subbands such that high-pass levels have higher frequencies and low-pass lower. As for the synthesis step, approximation and detail coefficients at the $j+1$ resolution scale can be found through signal interpolation by a factor 2, with zeros added between terms and subsequent convolution with filters $g_{lp}(n)$ and $g_{hp}(n)$. Filter bank implementation composed by this structure can be done with the algorithm (piramidal algorithm) developed in Mallat (1989) for the discrete WT. Figure 1 depicts how this WT implementation with filter banks work.

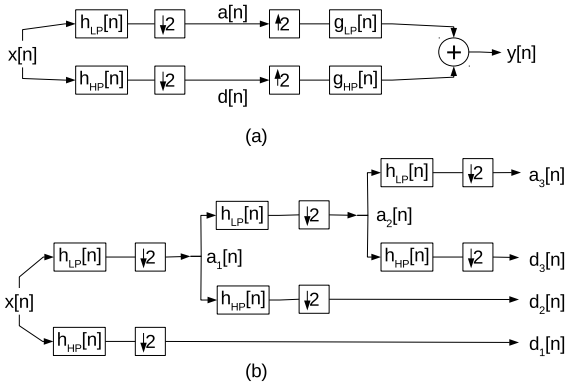

Figure 1: *WT implementation with filter banks. (a) Analysis and synthesis step at level 1. (b) Analysis step with filter banks at the third level.*

Selection of the appropriate filter bank for data compression is critical, once one having better ratio of loss-and-gains between the compression ratio, the signal reconstruction error and the total energy preserved may lead to better results. Following the results in Gomes et al. (2014) the chosen filter bank were the biorthogonal of class Cohen-Daubechies-Feauveau (CDF), 9/7, the same used in the JPEG image compression.

SPIHT Compression

In Said and Pearlman (1996) an extension of the Embedded zerotree wavelet (EZW) codec of Shapiro (1993) is presented as a faster and at the same time as having equal or superior performance, the SPIHT (Set Partitioning in Hierarchical Trees).

From the wavelet transform theory introduced above, it can be stated that low-pass levels (containing lower data frequencies) concentrate most of signal energy. Moreover, spatial similarities exist between subbands as exemplified in Salomon (2006): "An image part, such as an edge, occupies the same spatial position in each subband". These are the main properties exploited by wavelet compression methods as SPIHT, treated here.

SPIHT uses progressive transmission of the data, in a way that the most important data information is transmitted first. Selection by importance considers a mean squared-error distortion measure. Taking $\boldsymbol{A}$ and $\hat{\boldsymbol{A}}$ as the original and compressed data WT, respectively, and that the Euclidean norm is invariant to wavelet transformation the distortion measure is:

$$D_{mse} = \frac{\|A - \hat{A}\|}{number\ of\ elements}. \tag{4}$$

Using the above equation SPIHT will transmit the greater WT coefficients (considering an absolute value) first, ensuring that the compressed data contains the maximum signal energy, considering the bit threshold used, as possible and thereby the less distortion. This property will permit to flexibly control the compression rate (Zheludev et al., 2004).

Selection of larger WT coefficients needs sorting them in decreasing order while storing its position (ordering information) what would mean more data. SPIHT does not sort all coefficients, instead it selects the significant ones by partitioning the data set in subsets, which are created and partitioned using the called *spatial orientation tree* data structure. The latter defines a spatial relationship between subsets using the above mentioned similarity of subbands.

Seismic data compression using SPIHT first appears in Duval et al. (1999) followed by works as Zheludev et al. (2004) and more recently Xie et al. (2014). Considering the achieved results of SPIHT to seismic data reported in the literature, though not as rich as other gephysical research fields, good results have been reported.

Seismic Inversion

An inverse problem is one where information about a parameter is sought through an indirect measurement, a set of mathematical methods and physical relationships between the measurement method and the observed parameter.

A common classification of inverse problems is in well-posed or ill-posed where the matching of three conditions will tell in which of the two will a given problem be classified: (1) There exists a solution, (2) It is unique and (3) It is stable. The last being directly related to signal-to-noise ratio. If both conditions are satisfied, it is a well-posed problem, otherwise an ill-posed one.

Most geophysical problems are ill-posed, however an approximate solution may still be found through some regularization technique and/or use of *a priori* information. Here we treat the acoustic impedance inversion case where regularization usually assumes some kind

of sparsness to data as in Sparse-Spike methods, or prior information about the model can be added by using wells, from velocity analysis and by some constraining of the estimated model.

The mathematical method adopted to perform data inversion is Levenberg-Marquardt's algorithm (Levenberg, 1944; Marquardt, 1963) while the physical model is a linearization through Taylor series of the seismic data convolutional model. This combination is entitled Generalized Linear Inversion (GLI) in Cooke and Schneider (1983).

Considering a seismic pulse, W (source-signature) and a reflectivity series R from earth subsurface, through the convolutional model, the seismic signal, S will be generated by convolution of R and W.

The linearized model as a function of earth subsurface impedance Z and an initial guess $\hat{Z}$ is:

$$S(Z) = S(\hat{Z}) + \frac{\partial S(\hat{Z})(Z - \hat{Z})}{\partial \hat{Z}}. \quad (5)$$

The solution is sought iteratively through:

$$\hat{Z}_k = \hat{Z}_{k-1} + J_k, \quad (6)$$

where J_k refers to error in model estimation and will be calculated with Levenberg-Marquardt's method as:

$$J_k = (D_\partial^T D_\partial + \kappa I)^{-1} D_\partial^T [S(Z) - S(\hat{Z})], \quad (7)$$

with $D = \frac{\partial S(\hat{Z})}{\partial \hat{Z}}$, I as the identity matrix and κ described as a parameter associated to local linearity of the error surface.

RESULTS

The seismic volume before mentioned, is shown in figure 2.

Seismic data compression was applied to the data set considering the following reductions in bit per pixel representation: 0.25, 0.5 and 0.6. Three measures were used to analyze performance and therefore reconstruction quality: The Peak-Signal-to-Noise-Ratio (PSNR), the Percentual remaining energy (PE) and the Root Mean-Squared Error (RMS). Table 1 shows the computed measures considering each reduction plus the Percentual of Compression (PC), measuring the rate between compressed and real data.

Figures 3a, 3b and 3c shows the result of compression using the three thresholds for the inline 70. The trace shown in the figure is in the same coordinates as an used well.

A quantitative analyzis of compression from table 1 shows that small values for the RMS error were obtained while most of the energy was preserved. Also, the considerably high PSNR values means that noise related to

Table 1: *Compression Results.*

REDUCTION	068.25	0.5	0.6
PSNR (dB)	58.5251	61.4256	62.1783
PE	97.9%	98.59%	98.5%
RMS	102.8242	73.6322	67.5207
PC	0.39%	0.78%	0.94%

uncertainty in reconstruction is not as high as to destroy the original signal characteristics, in other words the reconstructed and uncompressed data have a good similarity in the sense that main features were preserved.

Analyzing the figures, similarity between uncompressed and compressed signals is easily seen. By a visual analysis, arthifacts are hardly found, thus the residual image in the leftmost part of figures shows a colored noise-like behaviour with most values ranging below 150.This feature of the residual image appears in the reconstructed image as an enhancement of correlated features (seismic reflections). Considering the SPIHT algorithm filters the higher frequency information it is expected that uncorrelated noise, to which this information is related, be filtered out.

For all seismic data compression thresholds, the inversion parameters were held the same as for the original data to evaluate how acoustic impedance is influenced by compression. Therefore, despite the following results, a search of better parameters to invert the compressed data will possibly lead to less uncertainty. The initial model for inversion was generated using three wells crossing the data as a means to guarantee better and more stable results.

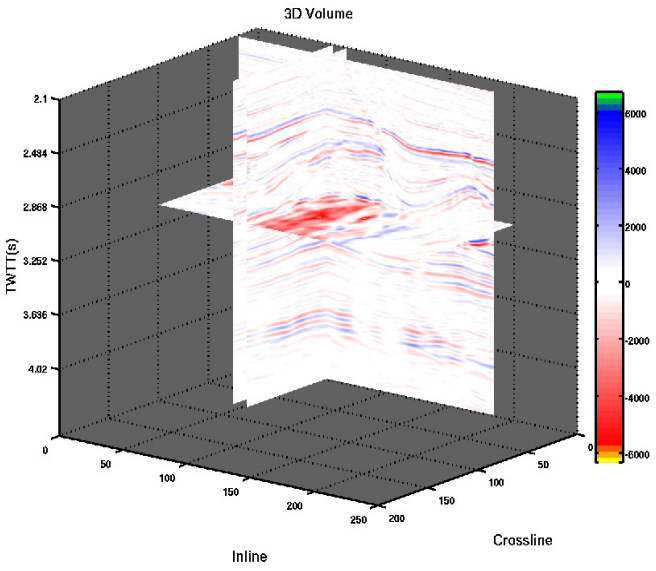

Figure 2: *Seismic volume.*

Table 2 shows the RMS error and PSNR measures

Table 2: *Inversion Results.*

REDUCTION	0.25	0.5	0.6
PSNR (dB)	22.0479	22.1229	22.1415
RMS	6.8541e+03	6.7952e+03	6.7807e+03

for the inversion results. RMS values are considerably higher than the compression results, though when looking at the value range of seismic and impedance data it can be noted impedances's values are higher. Nevertheless RMS value for inversion represents approximately 20% of the higher impedance value while the maximum residue value is near 39% of it, considering the 0.6 threshold (expected to have less uncertainty).

Through observation of figures 4a, 4b and 4c the discrepancy between estimated impedances is outstanding. In trace 156 shown in the figures, for time values of approximately 2.78s the residue starts to grow. This growth behaviour is related to the fact that well information only exists until around this time value to constrain the inversion. Furthermore, the residue image does not show, as in the compression analysis case, a noise-like behaviour, except at the upper left and rigth parts, showing coherency in the residue pattern and growing in amplitude with depth, what is coherent with the observations from trace 156.

In some way, the results of seismic inversion using compressed data are extremely dependent on constraining since noise from uncertaninty in reconstruction is present, leading to, possibly, unstable results.

CONCLUSIONS

Compressing seismic data using SPIHT achieves high compression rates while at the same time guarantees a good visual quality and a small RMS error, ensuring good similarity of the reconstructed with the original data.

For SPIHT as most of wavelet compression methods, redundant information related to noise is discarded such that significative features of the signal are enhanced, leading to increase in lateral continuity of seismic reflection, thus to augmentation in data quality.

However when aiming for inverson, even information considered as redundant will have its use. Results from compressed seismic data inversion shows that estimated impedances are highly dependent on constraining, here done through use of wells. Nevertheless there was a substantial difference between impendance estimates from uncompressed and compressed data even in regions where constraining was present.

For inversion results also, the main features were preserved when comparing with the estimate from original data, possibly as a result of main feature's preservation in seismic data. This property means that geological information about subsurface remains in the data even though compression makes it difficult to access.

The compression residue was observed to behave somewhat like colored noise. By considering the information about this residue can be predicted, obtained or estimated, and that it really is and always happens as uncorrelated noise, transmiting information about it would allow for noise addition in the inversion, much like prewhitening or an appropriate regularization, and therefore would assure more reliable impedance estimates.

ACKNOWLEDGEMENTS

Authors would like to thank PETROBRAS for the support to GISIS (Grupo de Imageamento Sísmico e Inversão Sísmica) from the Geology and Geophysics Department of Universidade Federal Fluminense.

REFERENCES

Burgos, R. B., M. A. C. Santos, and R. R. e Silva, 2013, Deslauriers–dubuc interpolating wavelet beam finite element: Finite Elements in Analysis and Design, **75**, 71 – 77.

Cooke, D. A., and W. A. Schneider, 1983, Generalized linear inversion of reflection seismic data: Geophysics, **48**, 665–676.

Duval, L. C., T. Q. Nguyen, and T. D. Tran, 1999, On progressive seismic data compression using genlot: Proc. Conf. Inform. Sciences Syst. (CISS), 956–959.

Gomes, V. M., M. A. Santos, D. L. F. Silva, R. B. Burgos, and D. M. S. Filho, 2014, Compressão wavelet con truncamento global para dados sísmicos: Presented at the VI Simpósio Brasileiro de Geofísica.

Khene, M., and S. H. Abdul-Jauwad, 2000, Adaptive seismic compression by wavelet shrinkage: Statistical Signal and Array Processing, 2000. Proceedings of the Tenth IEEE Workshop on, 544–548.

Levenberg, K., 1944, A method for the solution of certain non-linear problems in least squares: Quarterly Journal of Applied Mathmatics, **2**, 164–168.

Luo, Y., and G. Schuster, 1992, Wave packet transform and data compression: SEG Technical Program Expanded Abstracts, 1187–1190.

Mallat, S., 1989, A theory for multiresolution signal decomposition: the wavelet representation: Pattern Analysis and Machine Intelligence, IEEE Transactions on, **11**, 674–693.

Marquardt, D., 1963, An algorithm for least-squares estimation of nonlinear parameters: Journal of the Society for Industrial and Applied Mathematics, **11**, 431–441.

Mertins, A., 1999, Signal analysis: Wavelets, filter banks, time-frequency transforms and applications: John Wiley & Sons, Inc. (330 páginas).

Said, A., and W. A. Pearlman, 1996, A new, fast, and efficient image codec based on set partitioning in hierarchical trees: IEEE Transactions on Circuits and Systems for Video Technology, **6**, 243–250.

Salomon, D., 2006, Data compression: The complete reference: Springer. (xxvii+1092 páginas).

Shapiro, J. M., 1993, Embedded image coding using zerotrees of wavelet coefficients: Signal Processing, IEEE Transactions on, **41**, 3445–3462.

Vaidyanathan, P., 1993, Multirate systems and filter banks: Prentice Hall. Prentice Hall Signal Processing Series. (944 páginas).

Villasenor, J., B. Belzer, and J. Liao, 1995, Wavelet filter evaluation for image compression: Image Processing, IEEE Transactions on, **4**, 1053–1060.

Villasenor, J., R. A. Ergas, and P. L. Donoho, 1996, Seismic data compression using high-dimensional wavelet transforms: Data Compression Conference, 1996. DCC '96. Proceedings, 396–405.

Xie, K., Z. Bai, and W. Yu, 2014, Fast seismic data compression based on high-efficiency spiht: Electronics Letters, **50**, 365–367.

Zheludev, V. A., D. D. Kosloff, and E. Y. Ragoza, 2004, Compression of segmented 3d seismic data: International Journal of Wavelets, Multiresolution and Information Processing, **2**, 269–281.

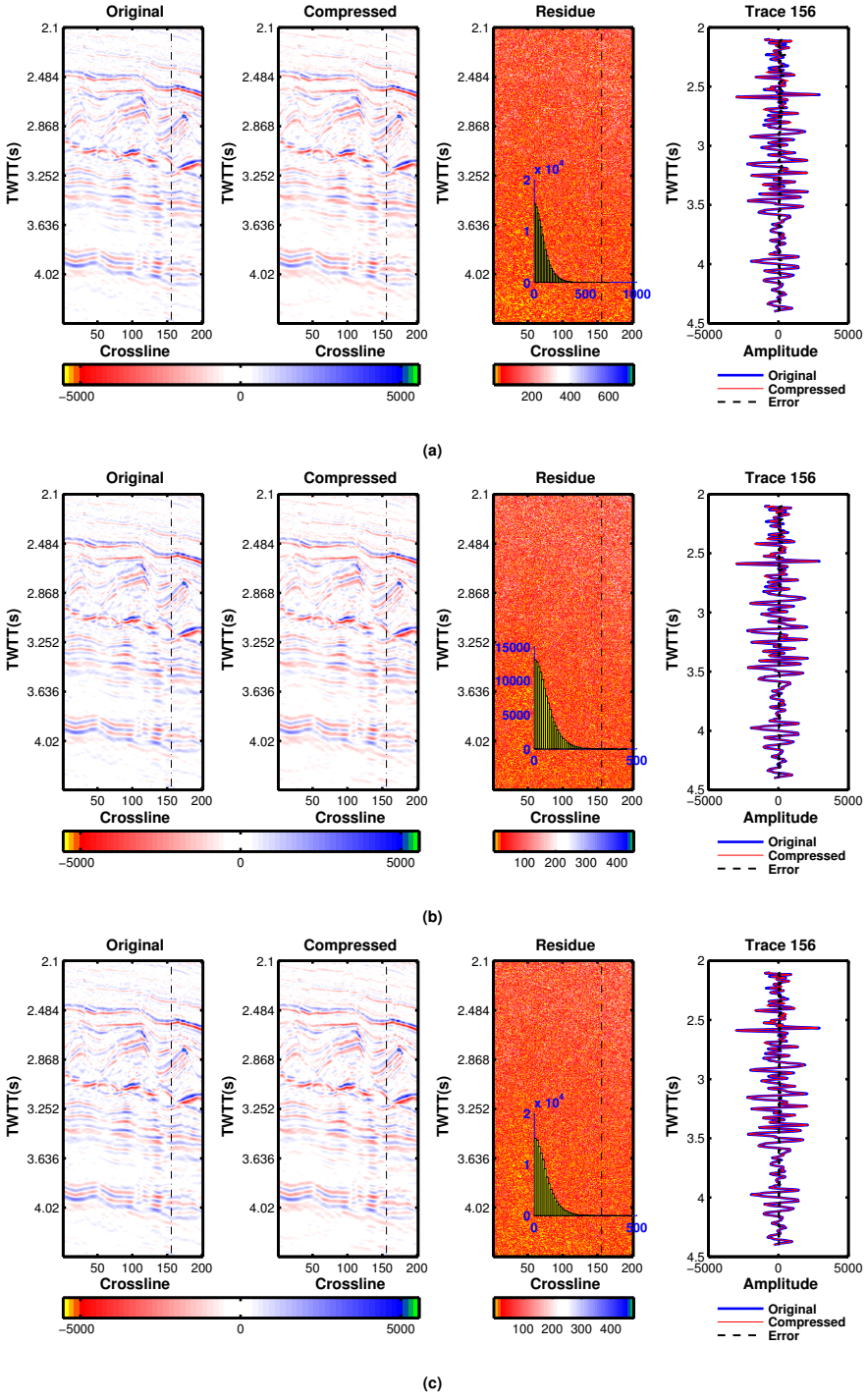

Figure 3: Comparison between real and compressed data considering a reduction to (a)0.25 (b)0.5 and (c)0.6 in the bit per pixel representation. Inline 70. Residue image has its histogram showing how values are distributed.

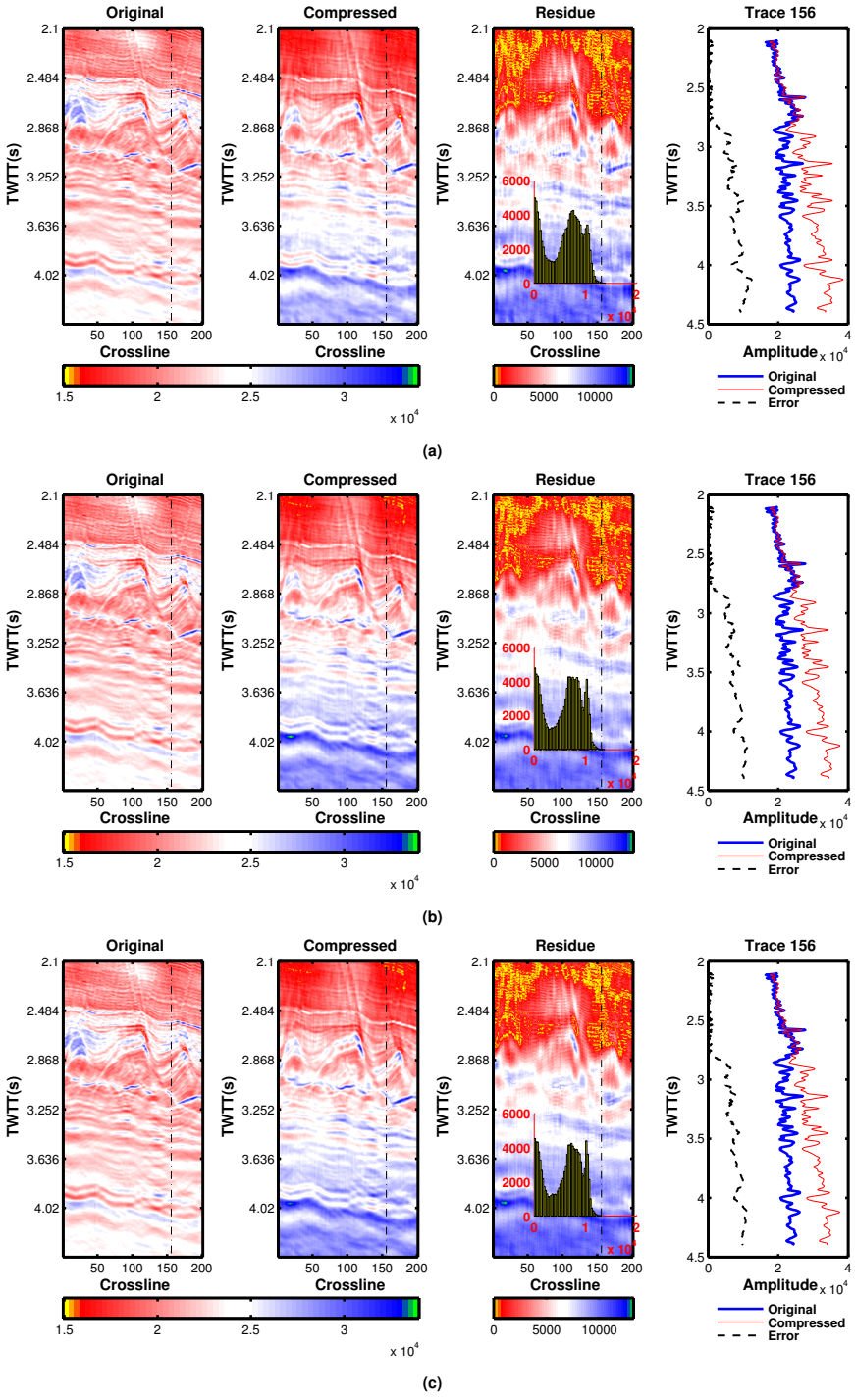

Figure 4: Comparison between estimated impedance from real and compressed data considering a reduction to (a)0.25 (b)0.5 and (c)0.6 in the bit per pixel representation. Inline 70. Residue image has its histogram showing how values are distributed.